JOURNAL OF SOLID STATE CHEMISTRY 97, 186–198 (1992)

Structure and Phase Transitions of Low-Dimensional Thallium Vanadium Bronze $Tl_xV_2O_5$ ($0.44 \leq x \leq 0.48$)

M. GANNE,[1] A. JOUANNEAUX, AND M. TOURNOUX

I.M.N., Laboratoire de Chimie des Solides, UMR CNRS 110, Université de Nantes, 2 Rue de la Houssinière, 44072 Nantes Cédex, France

AND A. LE BAIL

Laboratoire des Fluorures, URA CNRS 449, Université du Maine, 72017 Le Mans Cédex, France

Received November 15, 1990; in revised form September 23, 1991

$Tl_{0.48}V_2O_5$ belongs to the solid solution $Tl_xV_2O_5$ ($0.44 \leq x \leq 0.48$). Its crystal structure has been refined from X-ray powder diffraction data in space group $C2/m$. The framework of this lamellar compound is built up from double-sheet slabs of edge-sharing distorted octahedra, which can preferably be depicted as square pyramids. The highly polarizable Tl^+ cations adopt a nearly cubic coordination between these slabs. A detailed analysis of the π-bonds shows that the electrons d^1 are localized in the d_{xy}-orbital of vanadium ions V(1). The migration of these self-trapped but mobile electrons, via a hopping process, confers on $Tl_{0.48}V_2O_5$ the properties of a two-dimensional polaronic semiconductor 2D-(SC) between 165 and 655 K. Below 165 K, which can be viewed as a three-dimensional ordering temperature T_c^{3D}, transport properties are analyzed by considering that the small polarons progressively become trapped. This trapping, which is evidenced in E.P.R. data, allows one to explain, at least qualitatively, the spin-glass-like behavior observed in $Tl_{0.48}V_2O_5$. Between 655 and 710 K, this compound undergoes a phase transition either to a (SC) state or a metallic state. From the evolution of the conductivity curve, the (SC) state seems to be the most probable. However, because of the highly anisotropic nature of $Tl_{0.48}V_2O_5$ and since transport measurements have been performed on sintered powder samples only, a transition to a metallic state cannot be definitively excluded.

1. Introduction

Since the first works of P. Hautefeuille, who had observed the "rochage" phenomenon in the "vanadyl–vanadates" compounds (*1*), the study of vanadium bronzes has gained increasing interest in the last 30 years.

The first structural determinations have been performed by A. D. Wadsley for both β-$Na_xV_2O_5$ and $Li_{1+x}V_3O_8$ (*2*) and by S. Andersson for the silver bronze δ-$Ag_{1-x}V_2O_5$ (*3*). However, the systematic study of the bronzes $M_xV_2O_5$ (with M = Li, Na, K, Cu, Ag, Mg, Co, Ni, Zn, Ca, Cd, Pb, Al, Cr, Fe) has been carried out by P. Hagenmuller and co-workers, who have shown, in particular, that the nature of the obtained phases as

[1] To whom correspondence should be addressed.

0022-4596/92 $3.00

well as the homogeneity ranges could vary significantly according to the inserted cation M (*4–9*).

Some common features have been illustrated by A. Casalot in both $Cu_xV_2O_5$ and $Ag_xV_2O_5$ series: on the one hand, both α and β phases may exist, and on the other hand both ε-$Cu_xV_2O_5$ and δ-$Ag_xV_2O_5$ phases have a layered structure (*8–11*). Moreover, the structures of β-$Cu_xV_2O_5$ ($0.26 \leq x \leq 0.64$) and of ε-$Cu_xV_2O_5$ ($0.85 \leq x \leq 1$) have been determined (*12*). For this latter phase, in which the copper is monovalent, an interpretation of the electric and magnetic properties has been proposed (*13*).

At the same time, J. B. Goodenough has demonstrated, particularly in the β-$M_xV_2O_5$ bronzes, that the conduction occurs through small-polaron hopping, for which only the mobility is activated (*14*). This survey is not exhaustive, and more details are available in the article written by P. Hagenmuller (*15*).

As part of the general study of the ternary thallium–oxygen compounds, one of us has been interested in the thallium (I) vanadates and the bronzes $Tl_xV_2O_5$ (*16–18*). The main purpose of this study was to investigate a possible metallic behavior in these bronzes, in which the nearly alkaline behavior as well as the high polarisability of Tl^+ ion (α = 5.11 Å^3 (*19*)) could lead to possible modifications for the iono-covalence of the host lattice V_2O_5. From this investigation, it appeared that the steric factors remained dominant.

From an isothermal study carried out at 570°C, it was possible to obtain two well characterized phases:

(i) $Tl_xV_2O_5$ ($0.44 \leq x \leq 0.48$) is blue-black colored, of monoclinic symmetry, and exhibits some isotype relationships with ε-$Cu_xV_2O_5$ and δ-$Ag_xV_2O_5$ (*17, 18*).

(ii) $Tl_xV_2O_5$ ($0.92 \leq x \leq 1$) is black colored, and its crystal structure of tetragonal symmetry is related to those of $K_2V_3O_8$ (*20*) and $Tl_2V_3O_8$ (*21*).

To our knowledge, vanadium bronzes with large alkaline ions have not been studied extensively; only the structures of $Cs_{0.33}V_2O_5$ (*22, 23*), CsV_2O_5 (*24*), $Cs_{0.35}V_3O_7$ (*25*), and $Cs_2V_2O_{13}$ (*26*) have been determined. Therefore, investigations of the phase $Tl_xV_2O_5$ ($0.44 \leq x \leq 0.48$) come within this framework, and within the more general field of phase transitions in low-dimensional compounds. In this paper, we describe the structure of $Tl_{0.48}V_2O_5$ refined from X-ray powder diffraction data (Part 2), as well as the electric and magnetic properties of the solid solution (Part 3), whose interpretation will be given in Part 4.

2. Structure determination of $Tl_{0.48}V_2O_5$

2.1. Experimental

The thallium vanadium bronzes are obtained by a ceramic method which consists of a solid state reaction between stoichiometric amounts of $TlVO_3$, VO_2 and V_2O_5 according to

$$x\ TlVO_3 + x\ VO_2 + (1 - x)\ V_2O_5 \rightarrow Tl_xV_2O_5.$$

The ground mixture is pelleted and placed in a silica tube sealed under vacuum (or under nitrogen). The reaction occurs at 570°C for 12 hr. After it is quenched, the product is reground, repelleted, and reheated under the same conditions. The percentages of thallium (I) and of vanadium are determined by potentiometric techniques.

For the composition of $Tl_{0.45}V_2O_5$, a nearly congruent fusion is observed at 610°C by Differential Thermal Analysis. The needles obtained are very deformable and are not of sufficient quality for a structure determination by single-crystal methods. Nevertheless, a photographic X-ray study confirms the monoclinic symmetry of $Tl_{0.45}V_2O_5$ with the following cell parameters:

$$a = 11.59(1)\ \text{Å},\ b = 3.670(5)\ \text{Å},$$
$$c = 9.55(1)\ \text{Å},\ \beta = 101.0(1)°.$$

TABLE I

STRUCTURE AND PROFILE PARAMETERS FOR $Tl_{0.48}V_2O_5$ AT ROOM TEMPERATURE WITH STANDARD DEVIATION IN PARENTHESES

Atom	Site	x	y	z	B(Å^2)
Tl	$2d$	0	$\frac{1}{2}$	$\frac{1}{2}$	[a]
V(1)	$4i$	0.2079(4)	0	0.8447(4)	0.57(9)
V(2)	$4i$	0.0888(4)	0	0.1533(4)	0.57(9)
O(1)	$4i$	0.3745(11)	0	0.8726(10)	2.30(16)
O(2)	$4i$	0.0989(9)	0	0.3221(13)	2.30(16)
O(3)	$4i$	0.0603(12)	0	0.9063(11)	2.30(16)
O(4)	$4i$	0.2662(12)	0	0.1128(9)	2.30(16)
O(5)	$4i$	0.1738(10)	0	0.6832(13)	2.30(16)

Cell parameters: a = 11.609(8) Å, b = 3.6877(2) Å, c = 9.629(6) Å
β = 100.90(4)°
Space group: $C2/m$ (no. 14)
2θ range: 8–108°
Number of reflections: 289
Number of parameters: 35 (20 structural parameters)
Profile parameters (definition in (*32*)):

U_1 = 0.469(29)	V_1 = −0.0297(24)	W_1 = 0.173(5)	C = 0.0917(24)
U_2 = 0.0	V_2 = −0.178(55)	W_2 = 1.348(19)	D = −0.238(8)

R-factors: R_I = 5.48%; R_{wp} = 11.71%; R_{exp} = 5.87%.

[a] Anisotropic temperature factors for Tl atom:

β_{11} = 0.0054(3)	β_{22} = 0.0318(19)	β_{33} = 0.0064(3)
β_{12} = 0	β_{13} = 0.0002(2)	β_{23} = 0

The observed reflection condition $h + k = 2n$ leads to the possible space groups $C2/m$, $C2$, or Cm.

As one of us studied CDW–metal transitions in thallium molybdenum bronzes a few years ago (*27–29*), we have been therefore more interested in the limit composition $Tl_{0.48}V_2O_5$, whose particular electron/vanadium ratio close to $\frac{1}{4}$ could induce phase transitions driven by electronic instabilities at the Fermi level. Owing to the difficulty of obtaining single crystals, the structure was finally determined from X-ray powder diffraction data. The powder diffraction pattern was measured at room temperature on a conventional flat-plate Siemens D501 diffractometer equipped with a curve graphite post-sample monochromator using Cu$K\alpha$ radiation. As a strong preferred orientation effect was noted when the sample was packed on the holder, the diffraction pattern was finally obtained from a sample dusted on its holder through a 63-μm sieve. Data were collected in steps of 0.04° 2θ over the angular range 8° to 108° 2θ with a counting time of 16 sec per point. An unidentified impurity was detected in the pattern. However the most intense visible reflection of this extra phase is less than 2% of that of the major phase, and the presence of this impurity was supposed not to alter drastically the physical properties.

2.2. *Data Analysis*

The powder diffraction pattern was analyzed by the Rietveld method (*30*). The starting values for the atomic coordinates were deduced from the structural data of ε-$Cu_xV_2O_5$, whose cell constants are very

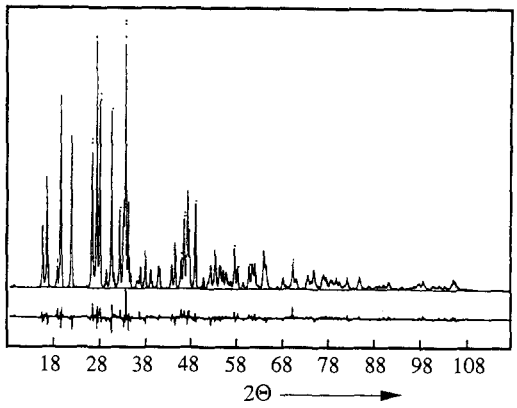

FIG. 1. Observed (...), calculated (−), and difference profiles for $Tl_{0.48}V_2O_5$.

close to those of $Tl_{0.48}V_2O_5$. The structure refinement was performed in the centrosymmetric space group $C2/m$ ($Z = 4$). Atomic scattering factors and anomalous-dispersion terms were taken from the "International Tables for X-ray Crystallography" (*31*). Isotropic B-factors were refined for all atoms but the heavy thallium ion, which was treated with anisotropic temperature factors. The Rietveld refinement converged to give the conventional R-factors: $R_I = 5.48\%$, $R_{wp} = 11.71\%$, and $R_{exp} = 5.87\%$ (calculated after background subtraction) for 289 reflections up to 108° 2θ. Despite the relatively high value of R_{wp} which is mainly due to preferred orientation residues, the structure is well determined overall. The final atomic coordinates and thermal parameters are reported in Table I, along with the profile parameters. The observed, calculated, and difference profiles are shown in Fig. 1. Further refinements in the noncentrosymmetric space groups $C2$ or Cm lead to no significant improvement.

2.3. Description of the Structure

A projection of the structure along the [010] axis is shown in Fig. 2. The structure consists of two types of very distorted VO_6 octahedra, which are linked by edges to form infinite chains in zigzag V(1)–V(2)–V(1)–V(2) . . . running along the **b** axis. The connection of these chains along the **a** axis through oxygen atoms O(3) leads to the formation of a sheet parallel to the (001) plane. Finally, the connection of two of these sheets through edge-sharing leads to the formation of slabs, which make up the framework of this bronze. The thallium atoms adopt a nearly cubic coordination between these slabs. From the values of the anisotropic temperature factors for the thallium, the main axes of the tensor nearly coincide with the three axes **a**, **b**, and **c***. Moreover, the long axis lies along **b**,

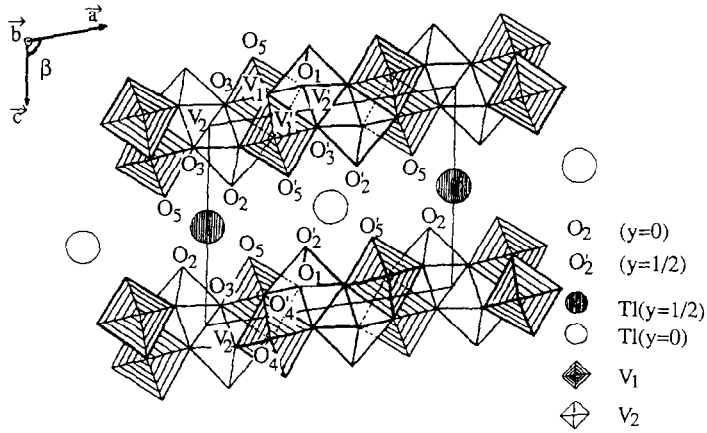

FIG. 2. Projection along [010] of the structure of $Tl_{0.48}V_2O_5$.

TABLE II

METAL–OXYGEN MAIN DISTANCES (Å) AND BOND ANGLES (°) IN $Tl_{0.48}V_2O_5$ WITH STANDARD DEVIATION IN PARENTHESES

V(1)	O(5)	O(4)	O(4)	O(1)	O(3)	O(4)
			$V(1)O_6$ octahedron			
O(5)	1.530(12)	2.688(8)	2.688(8)	2.674(15)	2.724(13)	4.072(15)
O(4)	102.7(7)	1.900(2)	3.688(12)	2.485(12)	2.763(14)	2.819(12)
O(4)	102.7(7)	152.0(6)	1.900(2)	2.485(12)	2.763(14)	2.819(12)
O(1)	101.8(12)	81.6(8)	81.6(8)	1.902(13)	3.724(18)	2.834(11)
O(3)	103.9(11)	92.7(7)	92.7(7)	154.4(11)	1.917(15)	2.806(16)
O(4)	179.6(9)	77.3(6)	77.3(6)	77.8(9)	76.6(9)	2.542(10)
V(2)	O(2)	O(3)	O(1)	O(1)	O(4)	O(3)
			$V(2)O_6$ octahedron			
O(2)	1.608(13)	2.591(15)	2.689(8)	2.689(8)	3.053(12)	3.945(16)
O(3)	102.3(13)	1.717(13)	2.809(14)	2.809(14)	3.760(19)	2.484(13)
O(1)	99.0(8)	101.0(8)	1.919(3)	3.688(11)	2.485(12)	2.810(12)
O(1)	99.0(8)	101.0(8)	147.8(7)	1.919(5)	2.485(12)	2.810(12)
O(4)	107.0(11)	150.7(11)	74.6(8)	74.6(8)	2.168(14)	2.806(16)
O(3)	176.1(10)	73.8(11)	82.0(7)	82.0(7)	76.9(10)	2.339(12)
			Tl–O distances < 4 Å			
		Tl–O(2) 2.897(10) [×4]		Tl–O(1) 3.039(9) [×4]		

which means that the displacements of the thallium are higher in this direction.

The metal–oxygen and metal–metal main interatomic distances are given in Tables II and III, respectively. From an analysis of the V–O distances, the distorted VO_6 octahedra may be best depicted as square pyramids, with a triple-bond character for the axial V–O bonds (V(1)–O(5): 1.530 Å; V(2)–O(2): 1.608 Å). Hence, the V_2O_5 slabs parallel to the (001) plane may be considered as weakly coupled double-sheet formed from edge-sharing square pyramids which point along the **c** axis in one sheet and in the opposite direction for the other. This description brings some simplification to the interpretation of electric and magnetic properties, which are reported in Parts 3 and 4.

TABLE III

METAL–METAL MAIN DISTANCES (Å) IN $Tl_{0.48}V_2O_5$ WITH STANDARD DEVIATION IN PARENTHESES

Vanadium atoms	
V(1)–V(1)	3.688(2) [×2]
–V(1)	3.492(4) [×2]
–V(2)	2.993(5) [×2]
–V(2)	3.448(5)
–V(2)	3.506(7)
V(2)–V(2)	3.688(2) [×2]
–V(2)	3.265(6)
Thallium atom	
Tl–Tl	3.688(2) [×2]
–V(1)	4.149(3) [×4]
–V(2)	4.112(5) [×4]

The framework of $Tl_{0.48}V_2O_5$ exhibits structural analogies with those of both δ-$Ag_xV_2O_5$ (*3*) and ε-$Cu_xV_2O_5$ (*12*). Similar layers of composition $(Ti_2O_5)_n$ are also present in the Wadsley bronze Na_xTiO_2, in which they are condensed along the **c** direction.

In Fig. 3 the projections along [010] of the idealized structures of the Wadsley bronze, of $Tl_xV_2O_5$, and of δ-$Ag_xV_2O_5$ are shown. The relative translation of the layers along the **a** axis enables the coordination of the inserted cation to be adjusted as well as pos-

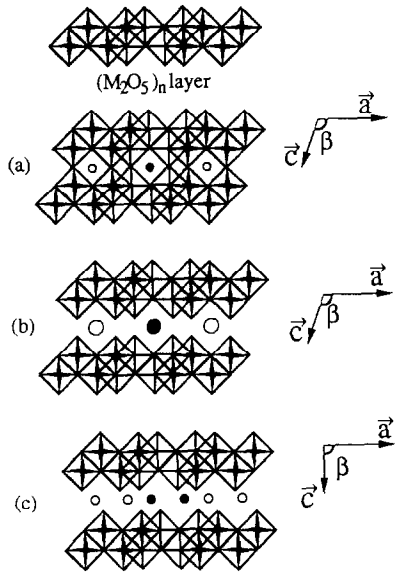

FIG. 3. Structural analogies of the idealized structures of $Na_{0.25}TiO_2$ (a), $Tl_xV_2O_5$ (b), and δ-$Ag_xV_2O_5$ (c).

sible, according to the cation size and its polarizability. Hence, the existence of these structural types as well as that of ε-$Cu_xV_2O_5$ suggests the possibility of synthesizing new intergrowth-phases involving the vanadium and/or titanium ions and some different size monovalent cations.

3. Physical Properties and Experimental Results

3.1. Transport Properties

Owing to the lack of single crystals, the electric conductivity measurements have been carried out for $Tl_{0.45}V_2O_5$ and $Tl_{0.48}V_2O_5$ on powder samples, sintered under primary vacuum at 550°C. For both samples, the density is very close to 90%. The measurements have been performed by two methods:

(i) a four-point direct current method using the Van der Pauw configuration (*33*). The contacts between the four gold wires and the sintered samples are made with gold lacquer.

(ii) a method using complex impedances for which we have used sintered pellets, whose faces had been gold plated under secondary vacuum (≈ 10^{-4} Torr).

Whatever the method used, the measurements, obtained in the temperature range 77–750 K, are in good agreement for $Tl_{0.48}V_2O_5$, which indicates that a possible ionic contribution to the conductivity due to thallium defects is very small. For the less stoichiometric compound $Tl_{0.45}V_2O_5$, the highest temperature of measurement was limited to about 500 K in order to avoid, a priori, ionic conductivity.

The evolution of log σ versus $10^3/T$ (K) is given in Fig. 4, for both compositions x = 0.45 and x = 0.48. These bronzes are semiconductors (SC) that exhibit a change in the activation energy at low temperature (210 K for $Tl_{0.45}V_2O_5$ and 165 K for $Tl_{0.48}V_2O_5$). The activation energy above the transition temperature is always smaller than below: for x = 0.45, the values above and below the transition temperature are 0.14 and 0.23 eV, respectively; for $Tl_{0.48}V_2O_5$, these values become 0.10 and 0.14 eV (the activation en-

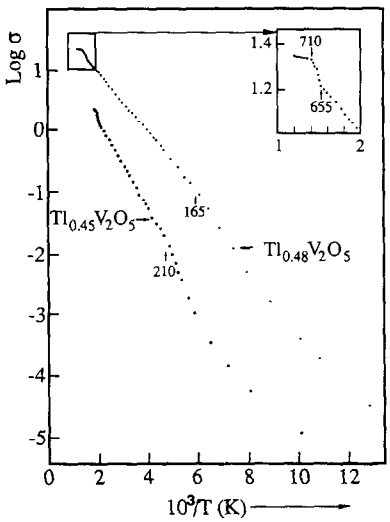

FIG. 4. Evolution of the conductivity vs ($10^3/T$) for $Tl_{0.45}V_2O_5$ and $Tl_{0.48}V_2O_5$.

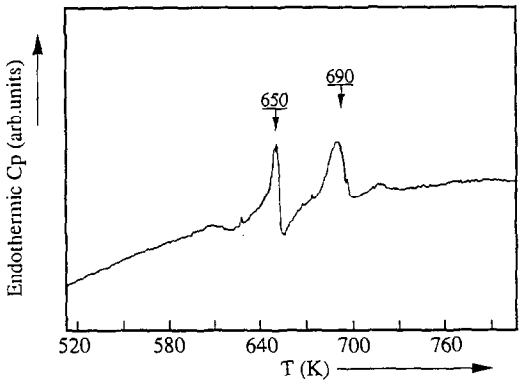

FIG. 5. Specific heat anomalies in $Tl_{0.48}V_2O_5$.

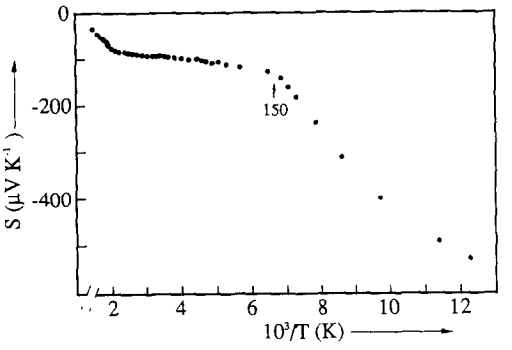

FIG. 6. Temperature dependence of the TEP in $Tl_{0.48}V_2O_5$.

ergy below the transition temperature is calculated from the straight portion of the curve).

By looking at these curves, it appears clearly that the conductivity is higher for the phase $Tl_{0.48}V_2O_5$, which is richer in carriers, than for $Tl_{0.45}V_2O_5$. It can be also noted that the difference between the activation energies, on either side of the transition temperature, decreases with increasing number of carriers.

For the composition $x = 0.48$, a reversible transition is also observed in the vicinity of 710 K (see inset in Fig. 4). This transition occurs between 655 and 710 K through a probable disordered state, which has been also suggested from a differential scanning calorimetric study. The measurement was performed with a temperature increase of 10 K/min between room temperature and 800 K. The result is shown in Fig. 5, where two reversible specific heat anomalies can be observed at 650 and 690 K for $Tl_{0.48}V_2O_5$. The transition enthalpies are 0.4 J/g and 0.8 J/g, respectively. For $Tl_{0.45}V_2O_5$, no such specific heat anomalies were detected.

The transport properties involve also thermoelectric power (TEP) measurements, which have been performed between 80 and 650 K by the symmetrical thermal gradients method (*34*) using two copper/constantan thermocouples applied with gold lacquer on each side of a sintered bar (length: 1 cm). The evolution of the TEP, measured on $Tl_{0.48}V_2O_5$, versus $10^3/T$ (K) is represented in Fig. 6.

It can be seen that the TEP is always negative, which indicates that the carriers are electrons. A nearly plateau behavior is observed from 500 down to 150 K. In the vicinity of this latter temperature, a discontinuity appears, which may be related to that which is observed at 165 K in the conductivity curve (Fig. 4).

3.2. Magnetic Properties

For $Tl_{0.45}V_2O_5$, the magnetic susceptibility measurements were carried out with a vibrating sample magnetometer (Foner) from 77 up to 300 K, and with a Faraday

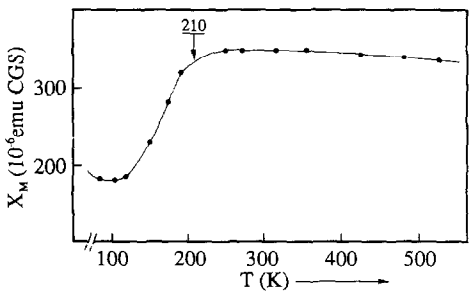

FIG. 7. Molar magnetic susceptibility vs temperature for $Tl_{0.45}V_2O_5$.

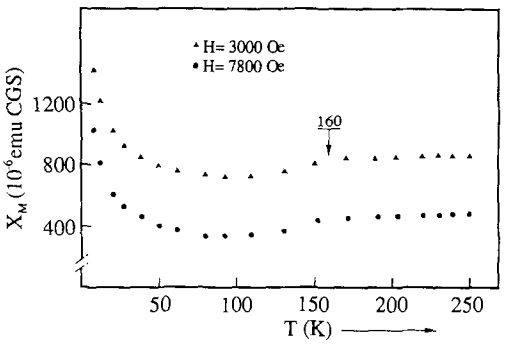

FIG. 8. Molar magnetic susceptibility vs temperature for $Tl_{0.48}V_2O_5$.

balance from room temperature up to 550 K. The temperature dependence of the molar susceptibility (corrected of core diamagnetism) is shown in Fig. 7.

For $Tl_{0.48}V_2O_5$, the magnetic susceptibility was measured with the help of a Faraday balance for various values of the applied magnetic field. In Fig. 8 are represented two curves $\chi_m(T)$ obtained for the following applied magnetic field values: 3 and 7 kOe. An anomaly can be observed in the vicinity of 160 K along with a decrease of the susceptibility with increasing applied magnetic field. This feature is reminiscent of spin-glass behavior.

This particular behavior is not observed in the less stoichiometric compound $Tl_{0.45}V_2O_5$. For this latter phase, a discontinuity appears in the vicinity of 210 K (Fig. 7); at this temperature, an anomaly exists in the conductivity curve as well (Fig. 4). Finally, for both compositions, the susceptibility is nearly constant beyond the transition temperature.

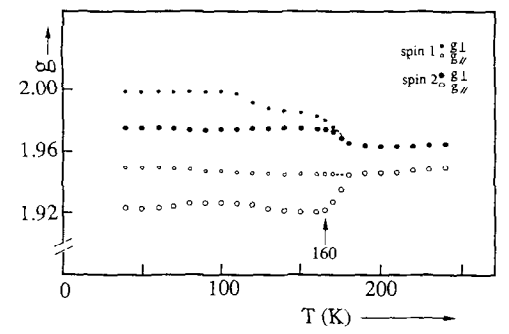

FIG. 9. Temperature dependence of the g-tensor values in $Tl_{0.48}V_2O_5$ measured by E.P.R.

For $Tl_{0.48}V_2O_5$, we have also undertaken an X-band E.P.R. investigation on powder samples from 10 up to 300 K. The detailed results of this study will be described elsewhere (*35*). The E.P.R. line whose halfwidth exhibits a marked discontinuity at 165 K has been fitted over the whole temperature range from a Gauss–Legendre integration procedure. From low temperature up to 165 K, two sites of axial symmetry, noted spin 1 and spin 2, are necessary to describe the E.P.R. signal. In Fig. 9, we show the temperature dependence of the components $g_\parallel$ and $g_\perp$ for both sites. Above 165 K, only one site becomes visible. This temperature corresponds to the discontinuity also observed for the susceptibility. From the E.P.R. simulations, we can also infer that the population of carriers for the site 1 is much greater than that of site 2.

4. Interpretation and Discussion

4.1. Introduction

In a vanadium oxide, the anionic p-orbitals are more stable than the d-orbitals centered at the metal; that is why it is possible to use the formal valence state of the ions to represent the number of d-electrons present per cation. Since the d-orbitals are antibonding with respect to the anionic p-orbitals, the cation–anion covalent mixing stabilizes the occupied p-states and simultaneously destabilizes the d-states. If the d-states are empty, the covalent mixing is increased, all the more so since the cation size is smaller. In this case, the cation tends to be displaced from the center of site symmetry, so as to favor the formation of π-bonding orbitals with the nearest neighbor anion, thus giving rise to multiple anion–cation bonds.

Since these localized π-bonds are hybridized with the anionic electrons, the corresponding d-orbitals are empty because of being destabilized. More generally, when a transition metal in an oxygen bronze has a mixed valence state, e.g., d^0-d^1 (V^V/V^{IV}; Mo^{VI}/Mo^V; W^{VI}/W^V), there the d^1-electron, located on an antibonding t_{2g}^* level, comes from the electronic transfer from the inserted metal (e.g., Na, Tl, Cu, etc.) to the oxide host-lattice. This transfer is complete as shown by the absence of an N.M.R. Knight-shift on the inserted metal nucleus.

According to the degree of delocalization of the t_{2g}^* level, the electron will be able to move either into a wide metallic band, as in the tungsten bronzes Na_xWO_3, or into a narrow metallic band, as in the molybdenum blue bronzes $K_{0.3}MoO_3$ or $Tl_{0.3}MoO_3$, or into a "localized" but still mobile state. This latter case is found in the vanadium bronzes, in which the electrons are considered as small polarons.

Because of a strong electron–phonon coupling in the vanadium bronzes, the time for an electron to jump from an occupied metal site to an empty site is long with respect to the period of longitudinal–optical phonon vibrations that assist the hopping process of these polarons (electrons self-trapped on their sites). Thus the charge carriers seem to be localized on time average. In the mixed-valent hopping regime, where the number of carriers is constant, only the very low mobility (≤ 1 cm^2/V sec) is activated.

From the conductivity curves for both compositions (Fig. 4), it can be deduced that the conduction is activated and is doubtless of polaronic type as in the other vanadium bronzes.

4.2. *Polaron Localization in* $Tl_{0.48}V_2O_5$

These polarons being d^1-centers, the value of the valence associated with such centers is equal to 4 for the corresponding V^{4+} ions. The value becomes equal to 5 for d^0-centers, i.e., V^{5+} ions formally. In the bronze $Tl_{0.48}V_2O_5$, the average valence is 4.76 for the vanadium ion. The application of the Zachariasen's law (*36*) with Brown's data (*37*) leads to valences equal to 4.91 for the vanadium V(1) and 4.61 for the vanadium V(2) if the six V–O distances of each distorted octahedron are taken into account. From this very simple calculation, the d^1-electron should be localized on the vanadium V(2).

However, a different conclusion can be reached regarding the t_{2g}^* orbitals when the vanadium polyhedra are viewed as slightly distorted square pyramids, as explained afore (2.3). The average distances for each pyramid are then 1.828 and 1.862 Å for the sites V(1) and V(2), respectively. Within each pyramid, the short distances V(1)–O(5) and V(2)–O(2) may be seen as triple bonds, which means that both d_{yz} and d_{xz}-orbitals, involved in the π-bonding orbitals, are empty initially. To accept the d^1-electron, the only available orbitals are then either the d_{xy}-orbital of V(1) or the d_{xy}-orbital of V(2). However, the rather short bond V(2)–O(3) (1.717 Å) corresponds to a double bond, for which the π-bonding orbital results from the overlap of the d_{xy}-orbital of V(2) with the p_y-orbital of the oxygen O(3). Therefore, the d_{xy}-orbital of V(2) is empty. On the other hand, the V(1)–O(3) bond is rather long with respect to the short V(2)–O(3) bond, and is comparable to the three other V(1)–O(1) and V(1)–O(4) [$\times 2$] bonds located in the (001) plane. This feature is consistent with the localization of the electron in the d_{xy}-orbital of the vanadium ion V(1). This result is confirmed by the g-values obtained from the E.P.R. investigation (Fig. 9). These values agree with spin resonance between the two Zeeman levels arising from the $\Gamma_7(B_2)$ ground state, deriving itself from the $^2B_2$ (d_{xy}) term in axial symmetry C_{4v}.

4.3. *Transport Mechanism in* $Tl_{0.48}V_2O_5$

By looking at the V–V distances given in Table III, the shorter distance (2.993 Å) corresponds to the intra-chain coupling V(1)–V(2)–V(1)–V(2) which runs along the **b** axis. This distance is slightly longer than the cation–cation critical distance R_c = 2.94 Å, below which Goodenough predicts a *d*-state delocalization through direct overlap (*38*). No strong coupling, even indirect, can exist between two V(1) sites (minimum distance: 3.492 Å) which do not belong to the same sheet of square pyramids. Inside a sheet, along the chains in zigzag V(1)–V(2)–V(1)–V(2), only the indirect coupling V(1)–O(4)–V(1) seems to be operative. This one occurs through d_{xy}–p_y–d_{xy} overlap because of the weakness of the σ-like bond V(2)–O(4) (2.168 Å). As pointed out by Goodenough, the V(1)–O(4)–V(1) interaction may give rise to a molecular-orbital state that causes this unit to be counted as a single site in the statistics used for the Seebeck voltage (*14*).

However, this static description does not take into account all the actual features. In particular, one has to consider the electron–phonon coupling effects, which can lead to a localization of states. For instance, increasing the *x*-coordinate of the oxygen O(3) (Fig. 2) causes the short bond V(2)–O(3) (1.717 Å) to relax and the long bond-length V(2)–O(4) to shorten via a strengthening of the σ-bond. This σ-bond involves mainly the p_x-orbital of the oxygen O(4), which substantially decreases the availability of the indirect coupling V(1)–O(4)–V(1).

At the same time, the bond V(1)–O(3) (1.917 Å) becomes shorter. These modifications, which are assisted by longitudinal-optical phonons, essentially favor the bidimensional hopping of small polarons.

In the temperature range 165 K $< T <$ 655 K, the number of charge carriers may be considered as constant, and only the mobility is activated, but all the electrons become mobile as the polaron–polaron interactions reduce the hopping activation energy. Below 165 K, according to the Seebeck voltage variation, the number of polarons available for conductivity decreases progressively. This reduction could be due to a possible formation of bipolarons, but because there is no evidence of a Néel temperature below 300 K and no collapse in the intensity of the E.P.R. signal as expected for spin-pairing in a bipolaron, we have to look for another explanation.

Superexchange interaction (double exchange is not operative for small polarons (*39*)) varies as the square of an interatomic overlap integral between t_{2g} orbitals, and the strength of this interaction varies exponentially with the V(1)–V(1) separation across a shared octahedral-site edge. A subtle structural change that modifies the V(1)–V(1) separation at 165 K would change χ_m for an "ordered" spin system by changing the strength of the exchange interaction. Indeed, a very weak specific heat anomaly (perhaps not significant and then not represented in this paper) covering a temperature range of 20 to around 150 K has been observed by DSC analysis. Furthermore, the E.P.R. data provide telling evidence for such a structural transition (Fig. 9). In terms of phase transition, T = 165 K may be considered as a three-dimensional ordering temperature T_c^{3D}. Below 165 K, excitation of polarons from trap sites rises the population of mobile polarons, and above a critical concentration, interaction between the mobile polarons can modify the structure so as to "free" all the polarons in the temperature range 165 K $< T <$ 655 K. Hence, spin-glass-like behavior, evidenced in magnetic data (Fig. 7), can be explained by considering trapped polarons in "ordered" domains.

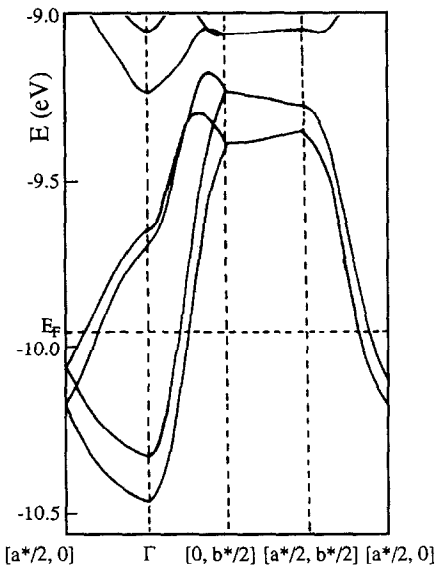

FIG. 10. Band structure calculated for a V_8O_{20} slab according to the tight-binding method (*40*).

Above 655 K, $Tl_{0.48}V_2O_5$ undergoes a phase transition (Fig. 4) via what is supposed to be a two-phase state revealed by the DSC analysis (Fig. 5), to a state which can be semiconducting (SC) or metallic. By looking at the conductivity curve, the transition seems to be of (SC) ↔ (SC) type. However, since the measurements have not been carried out on single crystals but on powder samples only and since the structure is highly anisotropic, a (SC) ↔ (Metal) transition cannot be definitively excluded. Indeed, some indirect arguments can be given in favor of such a transition: recent band calculations, performed on a V_8O_{20} slab in $Tl_{0.48}V_2O_5$ using tight-binding method (*40*) have shown that this compound is a quasi-two-dimensional metal at room temperature as far as electron–phonon interactions are not taken into account in the calculations (see Fig. 10). Its band pattern is very similar to that of Ti_8O_{20} of the Wadsley bronze $Na_{0.25}TiO_2$ (*41*) in which a 2D (SC) ↔ 1D (Metal) transition at 430 K has been recently demonstrated (*42*). In this latter compound, the transition to the metallic state is related to a slight shortening of the monoclinic **b** axis, as it could be the case in $Tl_{0.48}V_2O_5$. In addition, for both compounds, the (electron)/(transition metal) ratio is equal (or very close) to $\frac{1}{4}$. Since the electronegativity of V^V is higher than that of Ti^{IV}, a transition to the metallic state in $Tl_{0.48}V_2O_5$ may be expected at a temperature more than 430 K.

By looking at the Seebeck voltage curve of $Tl_{0.48}V_2O_5$ (Fig. 6), the TEP seems to be slightly activated in the plateau region; this is probably due to the granular texture of the sample. Although Heikes' formula (*43*), which is generally used to account for the Seebeck voltage in the hopping regime of small polarons, namely,

$$S = k/e \ln[(1 - c)/c], \text{ where } c = x/N,$$
$$\text{or } S = -198 \log[(N - x)/x](\mu V\ K^{-1}),$$

has not a rigorous statement (*44*); its direct application gives $S = -99\ \mu V\ K^{-1}$ using the values $x = 0.48$ and $N = 2$. This S-value is in rather good agreement with the experimental one ($S_{exp} \approx -100\ \mu V\ K^{-1}$). Nevertheless, when the unit V(1)–O(4)–V(1) is counted as a single site for evaluating N, as done by Goodenough in β-$M_xV_2O_5$ phases (*14*), the value $N = \frac{3}{2}$ is then obtained yielding $S = -65\ \mu V\ K^{-1}$, which is substantially different from the experimental value. In fact, the bond distances V(1)–O(4) are rather long (1.90 Å), and V(1)–O(4)–V(1) has perhaps not to be considered as a molecular unit. Otherwise, to account for the experimental Seebeck voltage, it would be necessary to invoke that only a polaron fraction is actually involved in the electronic transport.

5. Conclusion

The structure of the vanadium bronze $Tl_{0.48}V_2O_5$ has been solved from X-ray powder diffraction data in space group $C2/m$. The framework of this layered compound is built up from double-sheet slabs of composi-

tion $(V_2O_5)_n$. These slabs are similar to those of the layered bronzes δ-$Ag_xV_2O_5$ and ε-$Cu_xV_2O_5$. The originality of this thallium compound mainly depends on the size of the highly polarizable Tl^+ cations, which adopt a nearly cubic coordination between the slabs. Others large cations such as Rb^+ likely adopt such a coordination, and the study of the isotopic phase $Rb_xV_2O_5$ is now in progress.

Transport properties including conductivity and thermopower effect have been interpreted using a polaronic model. Small polarons are located in the t_{2g}^* "d_{xy}" orbital of vanadium V(1). Between 165 and 655 K, $Tl_{0.48}V_2O_5$ behaves like a 2D polaronic semiconductor. Below 165 K, which can be considered as a T_c^{3D} transition temperature, the small polarons become trapped. This trapping, which is demonstrated by an E.P.R. investigation and by the decrease of the Seebeck effect below 150 K, allows one to explain the spin-glass-like behavior evidenced on the magnetic susceptibility curves. Above 655 K, $Tl_{0.48}V_2O_5$ undergoes a transition, via what is supposed to be a two-phase domain, to a (SC) or a metallic state at 710 K. The semiconductor state, which seems to be the most probable, is however not proved definitively, owing to the lack of measurements performed on single crystals and to the highly anisotropic nature of this material.

References

1. P. Hautefeuille, *Compt. Rend.* (*Paris*) **90,** 744 (1880).
2. A. D. Wadsley, *Acta Crystallogr.* **8,** 695 (1955); **10,** 261 (1957).
3. S. Andersson, *Acta Chem. Scand.* **19,** 1371 (1965).
4. P. Hagenmuller, J. Galy, M. Pouchard, and A. Casalot, *Mater. Res. Bull.* **1,** 45 (1966).
5. P. Hagenmuller, J. Galy, M. Pouchard, and A. Casalot, *Mater. Res. Bull.* **1,** 95, (1966).
6. J. Galy, Thèse Doctorat, Université de Bordeaux (1966).
7. M. Pouchard, Thèse Doctorat, Université de Bordeaux (1967).
8. A. Casalot, Thèse Doctorat, Université de Bordeaux (1968).
9. J. Galy, M. Pouchard, A. Casalot, and P. Hagenmuller, *Bull. Soc. Fr. Mineral. Cristallogr.* **90,** 544 (1967).
10. A. Casalot, A. Deschanvres, P. Hagenmuller, and B. Raveau, *Bull. Soc. Chim. Fr.* **6,** 1730 (1965).
11. A. Casalot and M. Pouchard, *Bull Soc. Chim. Fr.* **10,** 3817 (1967).
12. J. Galy, D. Lavaud, A. Casalot, and P. Hagenmuller, *J. Solid State Chem.* **2,** 531 (1970).
13. A. Casalot, D. Lavaud, J. Galy, and P. Hagenmuller, *J. Solid State Chem.* **2,** 544 (1970).
14. J. B. Goodenough, *J. Solid State Chem.* **1,** 349 (1970).
15. P. Hagenmuller, "Comprehensive Inorganic Chemistry," Pergamon, New York (1973).
16. M. Touboul, M. Ganne, C. Cuche, and M. Tournoux, *Z. Anorg. Allg. Chem.* **1,** 1 (1974).
17. M. Ganne and M. Tournoux, *C.R. Acad. Sci.* (*Paris*) **273 C,** 975 (1971).
18. M. Ganne, Thèse Doctorat, Université de Nantes (1978).
19. J. Shanker and S. C. Agarwal, *Indian J. Pure Appl. Phys.* **14,** 79 (1976).
20. J. Galy and A. Carpy, *Acta Crystallogr., Sect. B: Struct-Crystallogr. Cryst. Chem.* **31,** 1974 (1975).
21. J. Tudo and B. Jolibois, *C.R. Acad. Sci.* (*Paris*) **273 C,** 466 (1971).
22. I. Lukacs, C. Strusivici, and C. Liteanu, *Rev. Roum. Chim.* **16,** 245 (1971).
23. K. Waltersson and B. Forslund, *Acta Crystallogr., Sect. B: Struct. Crystallogr. Cryst. Chem.* **33,** 780 (1977).
24. K. Waltersson and B. Forslund, *Acta Crystallogr., Sect. B: Struct. Crystallogr. Cryst. Chem.* **33,** 789 (1977).
25. K. Waltersson and B. Forslund, *Acta Crystallogr., Sect. B: Struct. Crystallogr. Cryst. Chem.* **33,** 775 (1977).
26. K. Waltersson and B. Forslund, *Acta Crystallogr., Sect. B: Struct. Crystallogr. Cryst. Chem.* **33,** 784 (1977).
27. M. Ganne, A. Boumaza, M. Dion, and J. Dumas, *Mater. Res. Bull.* **20,** 1297 (1985).
28. M. Ganne, M. Dion, A. Boumaza, and M. Tournoux, *Solid State Commun.* **59,** 137 (1986).
29. M. H. Whangbo, M. Evain, E. Canadell, and M. Ganne, *Inorg. Chem.* **28,** 267 (1989).
30. H. M. Rietveld, *J. Appl. Crystallogr.* **2,** 65 (1969).
31. "International Tables for X-ray Crystallography," Vol. IV, Kynoch Press, Birmingham (present distributor Reidel, Dordrecht) (1974).
32. A. Le Bail, H. Duroy, and J. L. Fourquet, *Mater. Res. Bull.* **23,** 447 (1988).

33. L. J. VAN DER PAUW, *Philips Res. Rep.* **13,** 1 (1952).
34. A. BONNET, P. SAID, AND A. CONAN, *Rev. Phys. Appl.* **17,** 701 (1982).
35. A. JOUANNEAUX, P. MOLINIE, AND M. GANNE, in preparation.
36. W. H. ZACHARIASEN, *J. Less-Common Met.* **62,** 1 (1978).
37. I. D. BROWN, *in* "Structure and Bonding in Crystals" (M. O'Keeffe and A. Navrotsky, Eds.), Vol. 2, p. 1, Academic Press, New York (1981).
38. J. B. GOODENOUGH, *Czech. J. Phys.* **B17,** 304 (1967).
39. J. B. GOODENOUGH, *in* "Defects and Transport in Oxides" (M. S. Seltzer and R. I. Jaffee, Eds.), p. 55, Plenum Press, New York (1973).
40. E. CANADELL, Private communication.
41. L. BROHAN, R. MARCHAND, AND M. TOURNOUX, *J. Solid State Chem.* **72,** 145 (1988).
42. M. EVAIN, M.-H. WHANGBO, L. BROHAN, AND R. MARCHAND, *Inorg. Chem.* **29,** 7 (1990).
43. R. R. HEIKES AND W. D. JOHNSTON, *J. Chem. Phys.* **26,** 582 (1957).
44. H. BOTTGER AND V. V. BRYKSIN, *in* "Hopping Conduction in Solids" (H. Böttger, Ed.), Akademie-Verlag, Berlin (1985).